Investigation Effect of ECR's Thickness and Initial Value of Resistance Spot Welding Simulation using 2-Dimensional Thermo-Electric Coupled

A.S. Baskoro
Mechanical Engineering Department, Universitas Indonesia

M.A. Amat
Mechanical Engineering Department, Universitas Indonesia

M.F. Arifardi
Mechanical Engineering Department, Universitas Indonesia

https://doi.org/10.5109/4742127

出版情報：Evergreen. 8 (4), pp.821-828, 2021-12. 九州大学グリーンテクノロジー研究教育センター
バージョン：

Investigation Effect of ECR's Thickness and Initial Value of Resistance Spot Welding Simulation using 2-Dimensional Thermo-Electric Coupled

A.S. Baskoro[1,*], M.A. Amat[1], M.F. Arifardi[1]

[1]Mechanical Engineering Department, Universitas Indonesia, Indonesia

*Corresponding Author's email: ario@eng.ui.ac.id

(Received April 30, 2021; Revised December 16, 2021; accepted December 16, 2021).

Abstract: The simulation of resistance spot welding (RSW) is used to approximate the experiment results and can be used to predict the nugget weld size. This article presents the 2D-Axisymmetric thermal-electric coupled model with properties of Electric Contact Resistance (ECR). The objective of his study is to investigate the effect of ECR thickness and the ECR's initial value on weld nugget geometry and thermal history. Direct current (DC) was applied with 10kA. Measurement of nugget geometry was performed by observing the temperature from the center of the weld through vertical and horizontal distribution. The result showed that the thickness of ECR and the ECR initial value significantly influenced the nugget temperature formation result.

Keywords: simulation; resistance spot welding; electric contact resistance; temperature

1. Introduction

While the development of various welding novelty is still competing, the resistance spot welding is still the best choice for the assembly process in the automotive industry [1)]. Compared to other welding methods, RSW is faster, maintainable, and can be automated [2)]. In the automotive industry, RSW is used to join parts of the vehicle structure. Mostly, it is made from aluminum in order to reduce fuel consumption caused by body mass [3)]. The market's demand of the aluminum in manufacturing industry has increased over years because of its lightweight, anti-corrosion, and mechanical-thermal properties [4)]. Moreover, it is used in wide range application like house, office, railways, bridge, and the aerospace industry [5-7)].

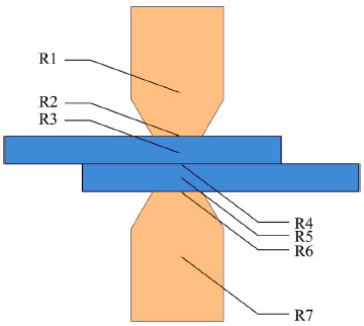

Fig. 1: Schematic of resistance spot welding

According to Ashtiani and Zarandooz [8)], the RSW process has some three types of physics phenomenon coupled interaction, which is difficult to analyze: thermal, electric, and metallurgical phenomena. Thus, making RSW simulation more complex and harder to get near an actual or experimental result. However, doing an experiment is an expensive and slow task when a large set of parameters is given. In other cases, simulation can work a dull task to find optimal parameters when time is limited and resources. By using Finite Element Method simulation, it will be effective to understand the experimental phenomenon to increase the accuracy of result [9)]. Therefore, RSW simulation is needed to find optimal parameters before doing an experiment for an economic purpose.

Joining aluminum is not an easy task because it has high thermal conductivity and electrical conductivity, high thermal expansion coefficient, low melting temperature, and the oxide layer formed on the top layer of aluminum surface [10)]. To achieve a good quality of weldment, some parameters significantly influence RSW nugget formation should be considered such as welding current, welding time, and electrode force [11-15)].

Fundamentally, the heat generated in the RSW process comes from the resistance components crossed by electrical current, as shown in Fig. 1 [16-17)]. RSW has two different types of resistance, and the first one is bulk resistance, which is shown by R1, R3, R5, and R7. The second resistance is contact resistance, which is shown by R2, R4, and R6 [18)]. The contact resistances are caused by the oxide or impurity layer between the contact surfaces based on their resistivity, roughness, and thickness [19)]. Therefore, electrical contact resistance (ECR) at the initial condition is high and gradually decreases as the metal is molten. The value of temperature-dependent ECR will affect the nugget formation [20)].

In this article, the RSW simulation was developed by using ANSYS MAPDL. The 2D axisymmetric model is used from previous work by Arifardi M. F [21]. This research was to investigate the effect of ECR thickness and the initial value of ECR on temperature distribution and then predicted the nugget geometry.

2. Method

Eq. (1) shows formula to calculate heat generation [8].

$$Q = I^2 Rt \tag{1}$$

Where Q [Joule], R [Ohm], I [Amp], and t [s] are heat, resistance, current, and time.

Table 1. Thermal properties of aluminum [1].

Temp (°C)	Ther. Exp. (10^{-6}/K)	Ther. Cond. (W/m/K)	Spec. Heat (J/Kg/K)	Dens. (kg/m^3)	Res. (μΩm)
20	22.0	192	885.8	2770	0.036
100	24.0	198	914.4		0.048
500	26.5	208	951.9		0.059
600	27.0	212	991.5		0.083
670	71.0	211	1033.1		0.095
800	65.0	205	1076.7		0.105
1000	60.0	98	1122.2		0.233
1200	56.0	100	1169.8		0.253

Table 2. Thermal properties of copper [22].

Temp (°C)	Ther. Exp. (10^{-6}/K)	Ther. Cond. (W/m/K)	Spec. Heat (J/Kg/K)	Dens. (kg/m^3)	Res. (μΩm)
21	16.6	390.6	397.7	8900	0.026
93	16.7	370.4	401.9		0.030
204	17.1	355.4	418.7		0.040
316	17.5	345.7	431.2		0.051
427	17.8	335.2	439.6		0.062
538	18.4	320.3	452.2		0.070
649	18.5	315.8	464.7		0.080
760	18.9	310.5	477.3		0.081
871	19.3	305.3			0.095
982	19.3	300.8			0.095

The full governing model was conducted in 2D-axisymmetric model in the cylindrical coordinate system. The heat balance equation is given by Eq. (2) [23].

$$\frac{1}{r}\frac{\partial}{\partial r}\left(kr\frac{\partial T}{\partial r}\right)+\frac{1}{r}\frac{\partial}{\partial z}\left(kr\frac{\partial T}{\partial z}\right)+\dot{g}=\rho c\frac{\partial T}{\partial t} \tag{2}$$

Where $\dot{g}$ refers to heat generation per unit volume, ρ is density [kg/m^3], c is specific heat capacity [J/(kg.K)] and k is thermal conductivity [W/(m.K)].

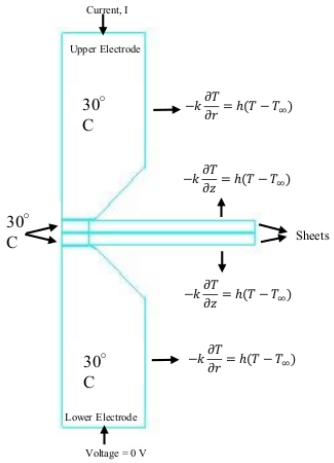

Fig. 2: Electric-thermal boundaries condition.

Table 1 and Table 2 show the temperature-dependent data of aluminum and copper's thermal properties, respectively. All boundaries condition is shown in Fig. 2. It is assumed that convection on all surfaces set constant 30 W/m^2, environment and initial temperature was set to 30°C. In this simulation there are two types of contact states: ECR Al-Al between aluminum sheets (R4) and ECR Al-Cu between aluminum and electrode (R2 and R6). The electric flow and heat generation was determined by these two contact states [24]. The value of electric contact resistance can be determined by Eq. 3 [25].

$$R_k(T)=\frac{\alpha R_0}{\beta^{(T-T_0)/(T_m-T_0)}} \tag{3}$$

Where $R_k(T)$ is the temperature-dependent contact resistance [Ohm], R_0 is the initial value ECR at room temperature [Ohm], α and β factor [Unitless] depending on the type of materials, T, T_0, and T_m are dependent temperature, environment temperature, and melting temperature [Celcius], respectively[24]. $R_k(T)$ is calculated based on $\alpha = 1$, $\beta = 10$, $T_0 = 30$°C, $T_m = 630$°C.

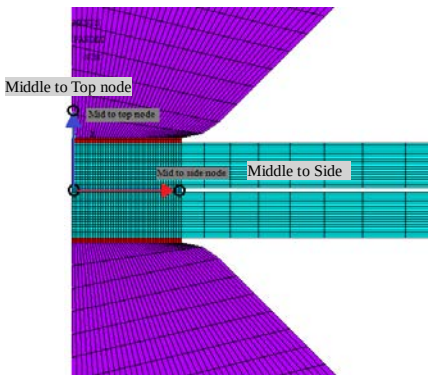

Fig. 3: Mesh scheme of the 2D-axisymmetric model and linear plots temperature in horizontal and vertical distribution.

As shown in Fig. 3, the aluminum thickness was set to 0.85 mm, and the electrode tip diameter was 4.08 mm. PLANE223 QUAD-8 node was used. The smallest mesh size for weld nugget zone was set to 0.1 mm, and the rest for others elements was set to 1 mm. The minimum time step required is 0.001s. Total amount duration was 200ms with 10kA current. The ratio of resistance (non-dimensional unit) of this study can be stated in Eq. 4.

$$Ratio = \frac{(R_0 \times thickness)_{Al-Al}}{2(R_0 \times thickness)_{Al-Cu}} \quad (4)$$

R_0 is the initial value resistivity. The ratio of resistance between $R_{Al\text{-}Al}$ and $R_{Al\text{-}Cu}$ was used as a point of analysis. The RSW simulation was carried out to investigate the effect of contact thickness and ECR's initial value at the interface between Al-Al and Al-Cu on weld nugget temperature distribution. Table 3 shows observations 1 and 2 with equal thickness. Table 4 shows observations 3 and 4 with an unequal thickness. Table 5 shows observations 5 and 6 with equal thickness.

Table 3. Variation of ECR's thickness with an equal contact thickness of $ECR_{Al\text{-}Al}$ and $ECR_{Al\text{-}Cu}$

Current (kA)	Observation 1		Observation 2		Thickness $ECR_{Al\text{-}Al}$ (μm)	Thickness $ECR_{Al\text{-}Cu}$ (μm)
	$ECR_{Al\text{-}Al}$ (μmΩ)	$ECR_{Al\text{-}Cu}$ (μmΩ)	$ECR_{Al\text{-}Al}$ (μmΩ)	$ECR_{Al\text{-}Cu}$ (μmΩ)		
10	300	50	150	150	10	10
10	300	50	150	150	20	20
10	300	50	150	150	30	30
10	300	50	150	150	40	40
10	300	50	150	150	50	50
10	300	50	150	150	60	60
10	300	50	150	150	80	80
10	300	50	150	150	100	100

Table 4. Variation of ECR's thickness with an unequal contact thickness of $ECR_{Al\text{-}Al}$ and $ECR_{Al\text{-}Cu}$

Current (kA)	Observation 3		Observation 4		Thickness $ECR_{Al\text{-}Al}$ (μm)	Thickness $ECR_{Al\text{-}Cu}$ (μm)
	$ECR_{Al\text{-}Al}$ (μmΩ)	$ECR_{Al\text{-}Cu}$ (μmΩ)	$ECR_{Al\text{-}Al}$ (μmΩ)	$ECR_{Al\text{-}Cu}$ (μmΩ)		
10	300	50	150	150	10	100
10	300	50	150	150	20	80
10	300	50	150	150	40	60
10	300	50	150	150	60	40
10	300	50	150	150	80	20
10	300	50	150	150	100	10

Table 5. Variation of ECR's initial value with an equal contact thickness of $ECR_{Al\text{-}Al}$ and $ECR_{Al\text{-}Cu}$

Current (kA)	Observation 5		Observation 6		Thickness $ECR_{Al\text{-}Al}$ (μm)	Thickness $ECR_{Al\text{-}Cu}$ (μm)
	$ECR_{Al\text{-}Al}$ (μmΩ)	$ECR_{Al\text{-}Cu}$ (μmΩ)	$ECR_{Al\text{-}Al}$ (μmΩ)	$ECR_{Al\text{-}Cu}$ (μmΩ)		
10	100	150	50	50	30	30
10	100	200	100	50	30	30
10	100	250	150	50	30	30
10	-	-	200	50	30	30
10	-	-	250	50	30	30
10	-	-	300	50	30	30
10	-	-	350	50	30	30
10	-	-	400	50	30	30
10	-	-	450	50	30	30
10	-	-	500	50	30	30

3. Results and Discussion

3.1 Contact Thickness Observation

Fig. 4 shows results from observation 1, which have an initial value of $ECR_{Al\text{-}Al}$ 300 µm.Ω and $ECR_{Al\text{-}Cu}$ 50 µm.Ω on all thickness variation. Both thicknesses are equal; therefore, all configurations have the same ratio number (ratio=3). Fig. 4a shows that the red contour is the formation of melting zone using thickness 30 µm, the geometry is to form an ellipse shape pointed at each end. The other temperature contour only shows the heat affected zone (HAZ) region. Therefore, the next explanation will be only focusing on the red contour which is the melting zone occurred. Fig. 4b shows the maximum temperature of all thickness variations and the red line is the critical line melting temperature. As the result shows the critical thickness is between 20-30µm, so 30 µm is the minimum thickness required to get aluminum reached above the melting point. Fig. 4c and Fig. 4d show temperature in a horizontal and vertical linear plot. It can be drawn to compare the width and height of the melting zone. As can be seen in the both figure increasing ECR thickness will result in bigger size melting zone and higher maximum temperature in center location.

Fig. 5 shows results from observation 2, which have an initial value of $ECR_{Al\text{-}Al}$ 150 µm.Ω and $ECR_{Al\text{-}Cu}$ 150 µm.Ω. All configurations have the same ratio number (ratio=0.5). Fig. 5a shows the red contour zone is the formation of melting zone with a thickness 40 µm and also can be said as the geometry of nugget tends to form like a shell or similar to a diamond shape. Fig. 5b shows the maximum temperature of all thickness variations. It has a lower maximum temperature compared to the observation 1. The result shows the critical thickness is at near 30 µm, which is the minimum thickness required to get aluminum reached above the melting point. Fig. 5c and Fig. 5d show that the horizontal and vertical plot, the plot figure is to show comparison of all variation thickness the width and height of the melting zone. And also show that the thickness above 30 µm would reach above the melting point.

Fig. 6(a-f) shows that the temperature formation field of RSW observation 3. As the ECR increased, the weld nugget zone will be increased. The parameter's resistivity ratios are 0.3, 0.75, 2, 4.5, 12, and 30, respectively. Temperature formation depends on the resistivity ratio. When it is less than 2, it tends to distribute in a diamond shape. Otherwise, it tends to distribute in ellipse shape. Fig. 7(a-f) shows the temperature formation fields of RSW observation 4. Similar to the observation 3, the weld nugget size is proportional to ECR and thickness. The resistance ratio of parameters are 0.05, 0.125, 0.334, 0.75, 2 and 5, respectively. When the ratio is less than equal to 0.334, it creates an axe shaped form. When the ratio is 0.75, it tends to form a diamond shape; otherwise, it will create an ellipse shape

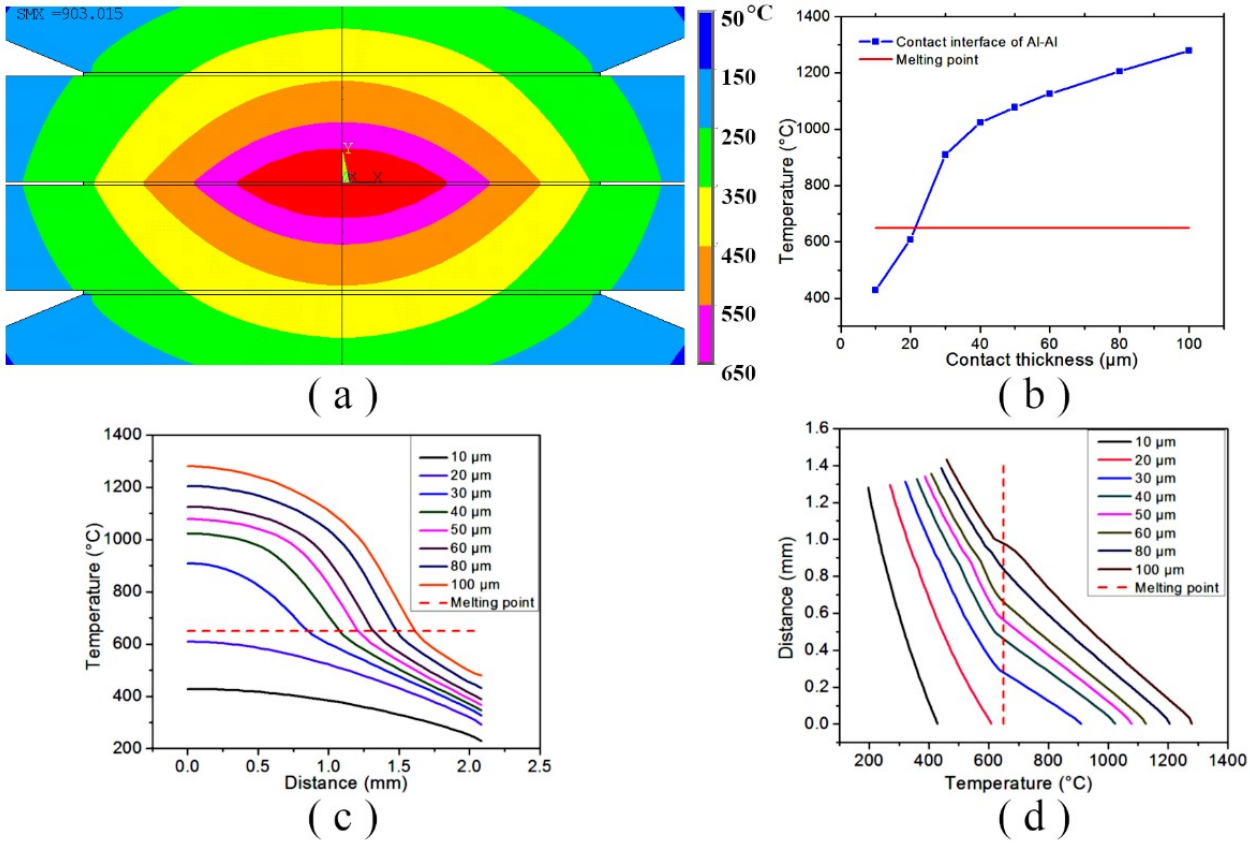

Fig. 4. (a) Temperature distribution of ECR thickness 30 µm with ratio=3. (b) Maximum temperature at the center node at various thicknesses. (c) Temperature distribution horizontally and (d) vertically at various contact thickness.

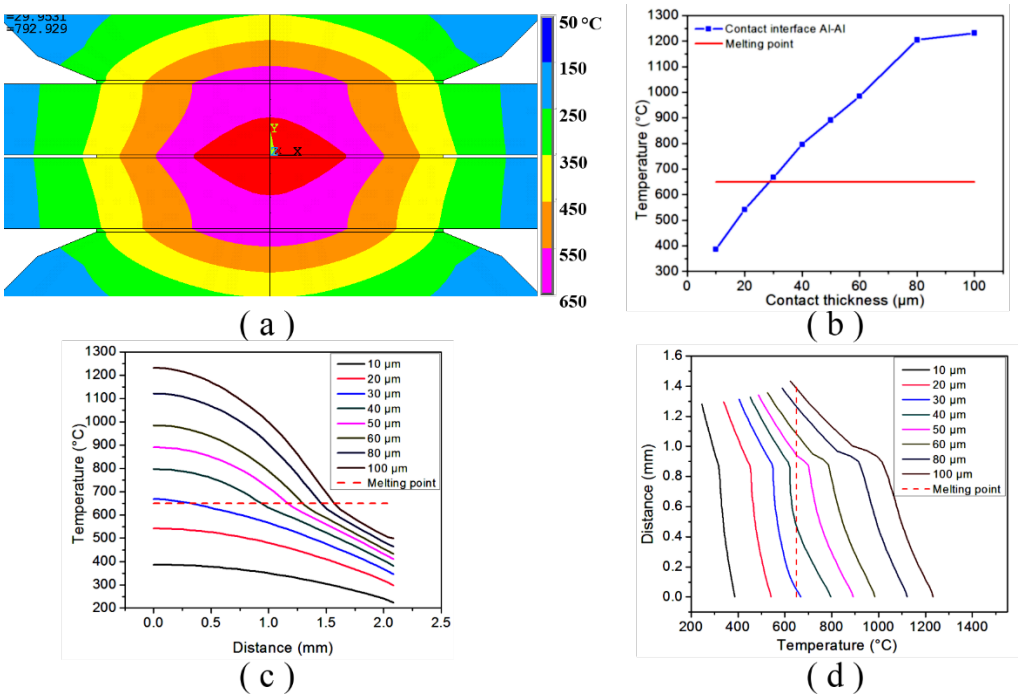

Fig. 5. (a) Temperature distribution of ECR thickness 40 μm with ratio=0.5. (b) Maximum temperature at the center node at various thicknesses. (c) Temperature distribution horizontally and (d) vertically at various contact thickness.

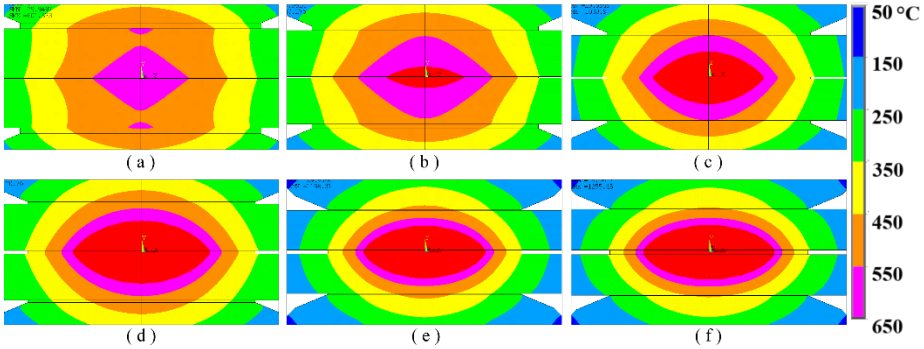

Fig. 6. Melting zone formation of contact thickness (a) Al-Al 10 μm and Al-Cu 100 μm, (b) Al-Al 20 μm and Al-Cu 80 μm, (c) Al-Al 40 μm and Al-Cu 60 μm, (d) Al-Al 60 μm and Al-Cu 40 μm, (e) Al-Al 80 μm and Al-Cu 20 μm, and (f) Al-Al 100 μm and Al-Cu 10 μm

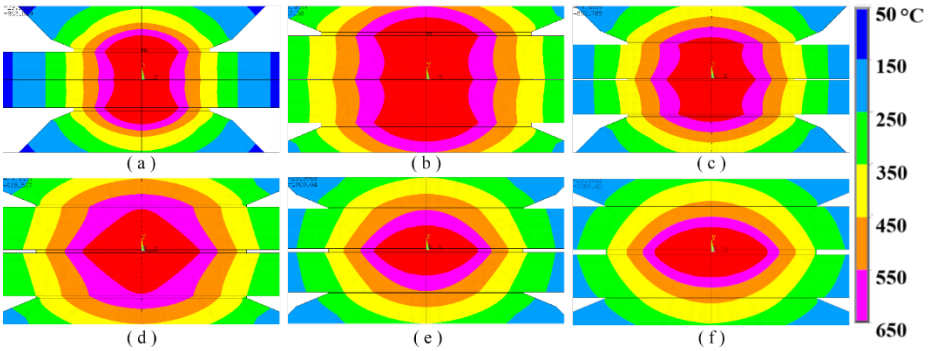

Fig. 7. Melting zone formation of contact thickness (a) Al-Al 10 μm and Al-Cu 100 μm, (b) Al-Al 20 μm and Al-Cu 80 μm, (c) Al-Al 40 μm and Al-Cu 60 μm, (d) Al-Al 60 μm and Al-Cu 40 μm, (e) Al-Al 80 μm and Al-Cu 20 μm, and (f) Al-Al 100 μm and Al-Cu 10 μm

3.2 ECR Initial Value Observation

The results of observation 5 are shown in Fig. 8(a-d). The contact thickness for Al-Al and Al-Cu is 30 µm. The resistivity ratio parameters are 0.334, 0.25, 0.2, and 2.5, respectively. Fig. 8 shows that the higher value of ECR_{Al-Cu} will make the heat generation concentrated more in the upper and lower sides than the center. Thus making the form diamond shape to an axe and finally form like a flower pot. Fig. 9 shows the result of simulation RSW observation 6. The contact thickness of Al-Al and Al-Cu is set constant to 30 µm. The resistance ratio is 0.5, 1.0, 1.5, and so on increased multiple by 0.5 points. Fig. 9a shows the melting zone formation goes in an ellipse shape. Fig. 9b shows by using 10 kA DC, the critical area lies between 200-250 µm.Ω. Therefore, the model needs ECR initial value Al-Al of more than or equal to 250 µm.Ω to reach above the melting point. Fig. 9c and Fig. 9d show the comparison of melting zone width and height, respectively, within various ECR value. It shows that the the ECR around 200-220 would reach the critical melting point.

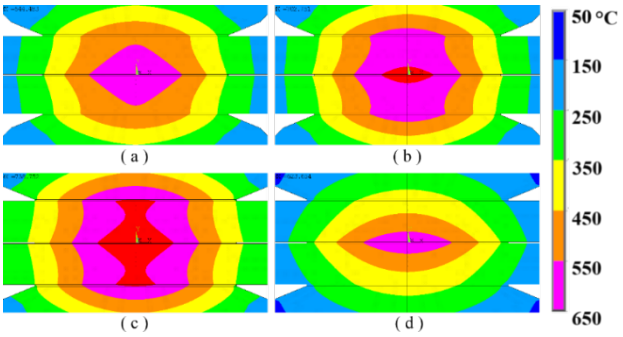

Fig. 8. Melting zone formation of (a) ECR (Al-Al 100 µm.Ω and Al-Cu 150 µm.Ω) with contact thickness 30 µm. (b) ECR (Al-Al 100 µm.Ω and Al-Cu 200 µm.Ω) with contact thickness 30 µm. (c) ECR (Al-Al 100 µm.Ω and Al-Cu 250 µm.Ω) with contact thickness 30 µm. (d) ECR (Al-Al 200 µm.Ω and Al-Cu 50 µm.Ω) with contact thickness 30 µm.

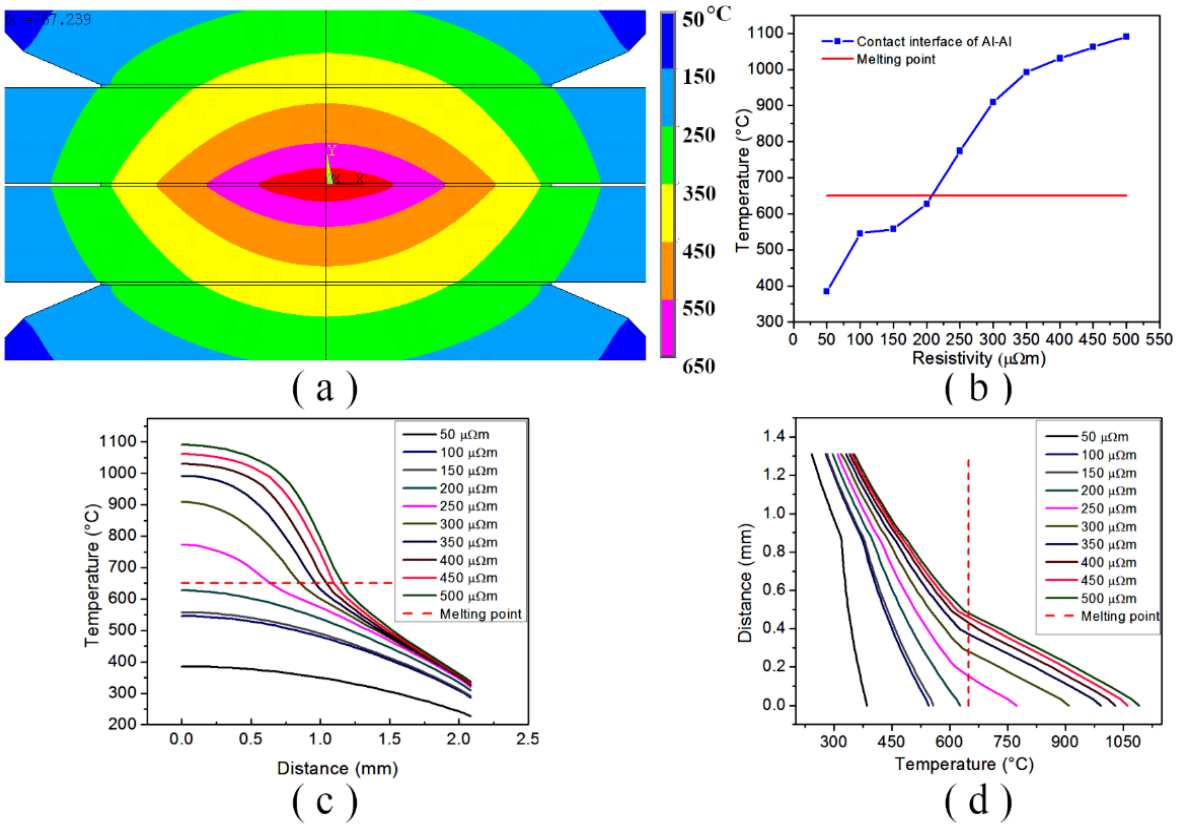

Fig. 9. (a) Temperature distribution of ECR (Al-Al 250 µm.Ω and Al-Cu 50 µm.Ω) with contact thickness 30 µm. (b) Maximum temperature at the center node at various thicknesses. (c) Temperature distribution horizontally and (d) vertically at various contact thickness.

4. Conclusions

The effect of ECR's initial value and contact thickness on temperature profile and nugget size for aluminum alloys has been studied using the finite element method. The conclusion can be drawn as follows; first, the weld nugget size depends on the ECR and current. By increasing the ECR, the weld nugget size will be increased. Second, the resistance ratio had a significant impact on the temperature formation shape. The resistance ratio of more

than 0.75, it tends to have an ellipse shape. The resistance ratio with less than 0.7 is less likely to be used because it tends to have a non-ellipse shape. In fact, the RSW experimental result will have a weld nugget with ellipse shape. Third, for the resistance ratio with more than 0.75, the nugget temperature distributes from the center weld area of Al-Al to the horizontal direction and slightly grows in a vertical direction. For future simulation, all parameters with a result of an ellipse weld nugget shape will be used as a reference.

Acknowledgements

Financial assistance for this work was granted by Directorate Research and Public Service, Universitas Indonesia, through the project of Hibah PITTA B with No: NKB-0706/UN2.R3.1/HKP.05.00/2019.

References

1) Z. Wan, H.-P. Wang, M. Wang, B.E. Carlson, and D.R. Sigler, "Numerical simulation of resistance spot welding of Al to zinc-coated steel with improved representation of contact interactions," *Int. J. Heat Mass Transf.*, **101** 749-763 (2016). doi:10.5109/2740953
2) C.V. Nielsen, W. Zhang, W. Perret, P.A. Martins, and N. Bay, "Three-dimensional simulations of resistance spot welding," *Proc. Inst. Mech. Eng. Part D J. Automob. Eng.*, **229** (*7*) 885-897 (2015). doi:10.1177/0954407014548740
3) J. Wang, H.-P. Wang, F. Lu, B.E. Carlson, and D.R. Sigler, "Analysis of Al-steel resistance spot welding process by developing a fully coupled multi-physics simulation model," *Int. J. Heat Mass Transf.*, **89** 1061-1072 (2015). doi:10.1016/j.ijheatmasstransfer.2015.05.086
4) A.K. Srivastava, S.P. Dwivedi, N.K. Maurya, and M. Maurya, "3D Visualization and Topographical Analysis in Turning of Hybrid MMC By CNC Lathe SPRINT 16TC Made of BATLIBOI," *Evergreen*, **7** (*2*) 202-208 (2020).
5) A.S. Baskoro, M.A. Amat, D. Putra, A. Widyianto, and Y. Abrara, "Investigation of Temperature History, Porosity and Fracture Mode on AA1100 Using the Controlled Intermittent Wire Feeder Method," *Evergreen*, **7** (*1*) 86-91 (2020). doi:10.5109/2740953
6) N. Mohd, M.M. Kamra, M. Sueyoshi, and C. Hu, "Three dimensional Free Surface Flows Modeled by Lattice Boltzmann Method: A Comparison with Experimental Data," *Evergreen*, **4** 29-35 (2017). doi:10.5109/1808450
7) M. Maurya, N.K. Maurya, and V. Bajpai, "Effect of SiC Reinforced Particle Parameters in the Development of Aluminium Based Metal Matrix Composite," *Evergreen*, **6** 200-206 (2019). doi:10.5109/2349295
8) H.R.R. Ashtiani and R. Zarandooz, "The influence of welding parameters on the nugget formation of resistance spot welding of inconel 625 sheets," *Metall Mat Trans A*, **46** (*9*) 4095-4105 (2015). doi:10.1007/s11661-015-3030-1
9) A. Yousefian and N. Yamamoto, "3D Finite Difference Time Domain Simulation of Microwave Propagation in a Coaxial Cable," *Evergreen*, **5** (*3*) 1-11 (2018). doi:10.5109/1957495
10) L. Deng, Y. Li, B.E. Carlson, and D.R. Sigler, "Effects of electrode surface topography on aluminum resistance spot welding," *Weld. J.*, **97** (*4*) 120s-132s (2018). doi:10.29391/2018.97.011
11) A.S. Baskoro, H. Muzakki, G. Kiswanto, and Winarto, "Effects of micro resistance spot welding parameters on the quality of weld joints on aluminum thin plate AA1100," *Int. J. Tech.*, **8** (*7*) 1306-1313 (2017). doi:10.14716/ijtech.v8i7.705
12) A.S. Baskoro, M.R. Trianda, J. Istiyanto, S. Supriyadi, D.A. Sumarsono, and G. Kiswanto, "Effects of welding time and welding current to weld nugget and shear load on electrical resistance spot welding of cold rolled sheet for body construction," *Int. Conf. Elec. Eng. Comp. Sci. (ICEECS)*, 289-293 (2014). doi:10.1109/ICEECS.2014.7045264
13) S. Aslanlar, A. Ogur, U. Ozsarac, E. Ilhan, and Z. Demir, "Effect of welding current on mechanical properties of galvanized chromided steel sheets in electrical resistance spot welding," *Mat. Des.*, **28** (*1*) 2-7 (2007). doi:10.1016/j.matdes.2005.06.022
14) S. Aslanlar, A. Ogur, U. Ozsarac, and E. Ilhan, "Welding time effect on mechanical properties of automotive sheets in electrical resistance spot welding," *Mat. Des.*, **29** (*7*) 1427-1431 (2008). doi:10.1016/j.matdes.2007.09.004
15) M. Eshraghi, M.A. Tschopp, M.A. Zaeem, and S.D. Felicelli, "Effect of resistance spot welding parameters on weld pool properties in a DP600 dual-phase steel: A parametric study using thermomechanically-coupled finite element analysis," *Mat. Des.*, **56** 387-397 (2014). doi:10.1016/j.matdes.2013.11.026
16) M. Hamedi and M. Atashparva, "A review of electrical contact resistance modeling in resistance spot welding," *Weld. World*, **61** (*2*) 269-290 (2017). doi:10.1007/s40194-016-0419-4
17) R. Raoelison, A. Fuentes, C. Pouvreau, P. Rogeon, P. Carre, and F. Dechalotte, "Modeling and numerical simulation of the resistance spot welding of zinc coated steel sheets using rounded tip electrode," *App. Math. Modell.*, **38** (*9-10*) 2505-2521 (2014). doi:10.1016/j.apm.2013.10.060
18) S. Manladan, F. Yusof, S. Ramesh, M. Fadzil, Z. Luo, and S. Ao, "A review on resistance spot welding of aluminum alloys," *Int. J. Adv. Manuf. Tech.*, **90** (*1-4*) 605-634 (2017). doi:10.1007/s00170-016-9225-9
19) P. Wei and T. Wu, "Electrical contact resistance effect on resistance spot welding," *Int. J. Heat Mass Trans.*,

55 (*11-12*) 3316-3324 (2012).
20) F. Cheng, J. Zhang, S. Hu, and P. Shan, "Numerical simulation on nugget formation and evolution in spot welding of aluminum alloy," *Trans. Tianjin Univ.*, **17** (*1*) 28-32 (2011). doi:10.1007/s12209-011-1517-4
21) M.F. Arifardi, A.S. Baskoro, and M.A. Amat, "Development of 2-dimensional finite element modeling of resistance spot welding: 1st generation model electric-thermal coupled," *AIP Conf. Proc.*, **2062** (*1*) (2019). doi:10.1063/1.5086584
22) Y. Li, J. Bi, Y. Zhang, Z. Luo, and W. Liu, "Shunting characteristics in triangular arranged resistance spot welding of dissimilar unequal-thickness aluminum alloys," *Int. J. Adv. Manuf. Tech.*, **91** (*5-8*) 2447-2454 (2017). doi:10.1007/s00170-016-9926-0
23) A. De, L. Dorn, and K. Momeni, "Probing the role of instantaneous current waveform in numerical modelling of resistance spot welding process," *Sci. Tech. Weld. Join.*, **10** (*3*) 325-334 (2005). doi:10.1179/174329305X40642
24) A. De, "Finite element modelling of resistance spot welding of aluminium with spherical tip electrodes," *Sci. Tech. Weld. Join.*, **7** (*2*) 119-124 (2002). doi:10.1179/136217102225002998
25) M. Greitmann and K. Rother, "Numerical simulation of the resistance spot welding process using spotwelder," *BOOK-INSTITUTE OF MATERIALS*, **695** 531-546 (1998). https://www.tib.eu/en/search/id/BLCP%3ACN027734889/Numerical-Simulation-of-the-Resistance-Spot-Welding/